Allocation of Peltier heating–cooling through the anomalous Hall effect

Aritra Ray,[1,2] Takamasa Hirai,[1,a)] Weinan Zhou,[1] Nanhe Kumar Gupta,[1] Yuya Sakuraba,[1] and Ken-ichi Uchida[1,3,a)]

[1] National Institute for Materials Science, Tsukuba 305-0047, Japan
[2] Indian Institute of Technology Guwahati, Guwahati 781039, India
[3] Department of Advanced Materials Science, Graduate School of Frontier Sciences, The University of Tokyo, Kashiwa 277-8561, Japan

[a)] Authors to whom correspondence should be addressed: HIRAI.Takamasa@nims.go.jp and UCHIDA.Kenichi@nims.go.jp

ABSTRACT

We report the observation of a spatial allocation of Peltier-effect-induced temperature modulation through the anomalous Hall effect (AHE) in a hybrid system comprising a magnetic metal and a thermoelectric semiconductor. AHE in the magnetic metal generates a transverse electric field perpendicular to the applied bias voltage, inducing charge injection into the thermoelectric layer via the closed circuit and resultant heating and cooling generation in a transverse geometry. Using an active thermal imaging technique, lock-in thermography, we visually extract the AHE-originating thermal contribution from other magneto-thermoelectric effects. Such heat allocation enables flexible design of transverse thermoelectric conversion, providing a pathway toward on-chip thermal management and selective temperature control at designated regions.

Thermoelectric technologies enable direct conversion between heat and electricity, allowing solid-state power generation and thermal management without moving parts or working fluids.[1–3] A classical thermoelectric phenomenon is the Seebeck effect,[4] in which a temperature gradient in a conductor generates a charge current through the coupled transport of heat and charge carriers [Fig. 1(a)]. The Peltier effect is the Onsager reciprocal of the Seebeck effect.[5] This phenomenon refers to the generation of the heat absorption or release at a junction between two conductors when a bias voltage drives a charge current flow across the interface [Fig. 1(b)]. Depending on the bias direction, the junction is cooled or heated, enabling active thermal management through electrical control. In these thermoelectric conversions, the charge and heat currents flow parallel to each other, hence they are called the longitudinal thermoelectric effects. Longitudinal thermoelectric devices, e.g., Peltier coolers and thermocouples, are witnessing rapid market expansion in temperature controlling and sensing applications; however, challenges remain in the mechanical and thermal durability and long-term reliability of modules that rely on complex π-type three-dimensional architectures.[6]

Recently, transverse thermoelectrics has attracted attention for overcoming such issues.[7–10] The transverse thermoelectric effects, which convert heat and charge currents in the orthogonal directions, provide a fundamentally different design paradigm for thermoelectric devices compared with the conventional Seebeck and Peltier modules. The Nernst effect, a representative transverse thermoelectric effect, generates a charge current perpendicular to both the temperature gradient and the magnetic field or magnetization. It is classified into the ordinary and anomalous components, corresponding to contributions from external magnetic fields and spontaneous magnetization, respectively. Recently, several thermoelectric generators and sensors based on the Nernst effect have been proposed, featuring simple, versatile, and flexible geometries without the need for complex structure.[11–21] The reciprocal of the Nernst effect is known as the Ettingshausen effect, in which a transverse temperature gradient is generated in the cross-product direction of a charge current and a magnetic field or magnetization. By exploiting this effect, one can actively control positions of heating and cooling through magnetic-field or magnetization manipulation without changing the bias direction,[22–24] offering another route toward thermoelectric thermal management. In 2021, Zhou *et al.* proposed another transverse thermoelectric conversion: the Seebeck-effect-driven anomalous Hall effect (AHE) in hybrid stacks comprising a thermoelectric material and magnetic conductor.[25] When a temperature gradient is applied to a closed circuit consisting of such two materials, a charge current flows in the circuit due to the Seebeck effect and this charge current is in turn converted into a transverse electric field due to AHE, $\mathbf{E}_{\mathrm{AHE}}$, in the perpendicularly magnetized magnetic conductor [Fig. 1(c)]. Since Seebeck-effect-driven AHE produces a transverse voltage with the same direction as the anomalous Nernst effect in the magnetic layer, it can realize a transverse thermopower exceeding that obtainable in a single magnetic material.[25–27] In analogy with the relationship between the Seebeck and Peltier effects and between the Nernst and Ettingshausen effects, the inverse process of Seebeck-effect-driven AHE could offer unconventional temperature-control capabilities for thermal management, but it has not yet been observed experimentally.

In this study, we report the experimental observation of the inverse process of Seebeck-effect-driven AHE, i.e., the AHE-driven Peltier effect, by means of an active thermal imaging technique called lock-in thermography (LIT). Figure 1(d) shows a concept of AHE-driven Peltier cooling–heating in a magnetic/thermoelectric hybrid stack. When a bias voltage is applied to the perpendicularly magnetized magnetic conductor, $\mathbf{E}_{AHE}$ emerges and the transverse charge current, $\mathbf{J}_A$, flows into the thermoelectric material. The injected charge current results in the Peltier-effect-induced heating or cooling at the junctions, the positions of which are far away from those of the conventional Peltier heating or cooling induced by a longitudinal charge current. Such heat allocation will open a route for on-chip thermal management with high spatial resolution, enabling the cooling of local hot spots and the redistribution of dissipated thermal energy. Moreover, it allows selective temperature control, which leads to tailor local functionalities and enhance device performance, thereby extending the role of AHE into active spintronic thermal management.

For this proof-of-concept, we used a Co/Pt multilayer film as the magnetic conductor and an *n*-type Si substrate as the thermoelectric material in the hybrid stack. The surface of the Si substrate is thermally oxidized; the SiO_x layer electrically insulates the deposited Co/Pt film from Si. By making electrical contact holes at the ends of the magnetic and thermoelectric layers, the AHE-induced transverse charge current can flow at the junctions and consequently generate the Peltier cooling/heating. Therefore, here we selected a thin-film-based device and followed the fabrication method for closed-circuit structures established in the previous research.[28] The Co/Pt multilayers exhibit sizable AHE[29–33] and large perpendicular magnetic anisotropy originating from the Co/Pt interfaces,[34,35] enabling the generation of AHE-induced transverse charge current without the need for an external magnetic field.

Figure 2(a) shows the device structure used in this study. First, a 0.5-mm-thick phosphorous-doped *n*-type Si substrate (hereafter, Si substrate) with a 100-nm-thick SiO_x insulating layer was cut into a chip of 10 mm square. Note that this Si substrate is the same one used in the previous study on Seebeck-effect-driven AHE; its electrical resistivity is 8.6 Ωcm and the Seebeck coefficient is about −1300 μV/K.[25,28] Subsequently, two contact holes were fabricated using photolithography and Ar-ion milling; we etched away two patches of the SiO_x layer with a size of 0.3×0.3 mm^2 area and 5.0 mm spacing between their centers, and then the holes were filled with Ta(2 nm)/Au(100 nm) layers by rf sputtering without breaking the vacuum. Finally, a cross-shaped Pt(0.6 nm)/[Co(0.4 nm)/Pt(1.2 nm)]$_n$ multilayer film (hereafter, [Co/Pt]$_n$ multilayer with n being repetition number) was fabricated on the substrate by a lift-off process using rf magnetron sputtering, where the wire along the y (x) direction has a length of 9.2 mm (6.0 mm) and width of 1.0 mm (0.5 mm). To investigate magnetic properties of [Co/Pt]$_n$ multilayers, we also prepared a Hall bar of the [Co/Pt]$_n$ multilayers with a width of 2 mm and a length of 7 mm on an SiO_x/Si substrate and performed the Hall measurements. As shown in Fig. 2(b), the saturation value of Hall resistivity ρ_{yx}, i.e., anomalous Hall resistivity, and coercivity were changed depending on the n value. Based on these results, the [Co/Pt]$_{12}$ multilayer, which exhibits the large anomalous Hall resistivity (1.57×10^{-6} Ωcm) with corresponding anomalous Hall angle (3.7%), squareness close to unity, and highest coercivity among the three multilayers, was selected for the observation of AHE-driven Peltier cooling/heating.

The temperature modulation in our device was measured using LIT.[36] LIT is an active thermal imaging technique that detects temperature responses induced by a periodically modulated external excitation with high temperature resolution,[37–43] To investigate thermoelectric responses, we acquired thermal images of the surface of the device using an infrared camera while applying a square-wave-modulated ac charge current $\mathbf{I}_c$ with amplitude I_c, frequency f, and zero dc offset in the y direction and obtained the first harmonic response of the thermal images. This procedure allows us to extract pure thermoelectric response free from Joule heating since thermoelectric and Joule-heating signals are proportional to I_c and I_c^2, respectively [Fig. 2(d)]. The extracted images were transformed into the lock-in amplitude A and phase ϕ through Fourier analysis, where A (ϕ) images give information on the magnitude of the temperature modulation (the sign of the temperature modulation and time delay due to thermal diffusion). During the LIT measurements, the device temperature was controlled around 310 K using a commercial thermoelectric module (see supplementary material S1) to supress the steady-state temperature rise caused by Joule heating and eliminate its I_c-dependent variations. To enhance the emissivity of the infrared radiation and its uniformity, the device surface was coated with insulating black ink whose emissivity is greater than 0.94.

Figure 2(e) shows the A and ϕ images at I_c = 80 mA and f = 25.0 Hz when **M** aligned along the $+z$ (top panels) and $-z$ (bottom panels) directions, where the direction of **M** was controlled by bringing a permanent magnet (its stray field >1 T) close to the device. Depending on the **M** direction, A values remain unchanged while ϕ sign is reversed, which is a feature of the magneto-thermoelectric effects. The signals were observed at two characteristic locations: the edges of the y direction of the wire and the contact holes [L and R in Fig. 2(c)], where the position of the contact holes was identified from the steady-state thermal image [Fig. 2(c)]. LIT images also visually confirm that there was no spurious thermoelectric signal arising from electrical shunting caused by pinholes or defects in the SiO_x layer, indicating that $\mathbf{I}_c$ primarily flows along the y-direction of the Co/Pt multilayer.

Thereafter, to thoroughly analyze the LIT signals dependent of the **M** direction, we extracted the **M**-odd-dependent component (referred to as A_{odd} and ϕ_{odd}) of the temperature modulation following the equations of $A_{odd} = |A(+M)\exp[-i\phi(+M)] - A(-M)\exp[-i\phi(-M)]|/2$ and $\phi_{odd} = -\arg\{A(+M)\exp[-i\phi(+M)] - A(-M)\exp[-i\phi(-M)]\}$, where $A(+M)$ [$\phi(+M)$] and $A(-M)$ [$\phi(-M)$] indicate A (ϕ) measured when **M** aligns along the $+z$ and $-z$ directions, respectively. Figure 3(a) shows the A_{odd} and ϕ_{odd} images extracted from two A and ϕ images in Fig. 2(e). The red (~0°) [blue (~180°)] region on the ϕ_{odd} images indicates the temperature increase (decrease), i.e., the heat release (absorption) at the left (right) edge of the wire and contact hole L (R) under a charge current along the $-y$ direction. Here, the observed LIT signals likely contain contributions from two magneto-thermoelectric effects: the AHE-driven Peltier effect and anomalous Ettingshausen effect (AEE). The latter contribution, AEE, generates a heat current in the direction of the cross product of $\mathbf{I}_c$ and **M** in magnetic conductors. Owing to the positive anomalous Nernst/Ettingshausen coefficient of Co/Pt systems,[44] the AEE-induced heat current $\mathbf{J}_{q,AEE}$ in the Co/Pt multilayer points along the $-x$ direction for the configuration in which $\mathbf{I}_c$ is along the $-y$ direction and **M** is along the $+z$ direction, which can explain the temperature increase (decrease) signal at the left (right) edge of the wire. To examine the origin of the signals at the contact holes, a control LIT experiment was conducted using a device of the cross-shaped $[Co/Pt]_{12}$ multilayer on the SiO_x/Si substrate without contact holes, in which the Si and Co/Pt layers are electrically isolated by the insulating SiO_x layer. As shown in Fig. 3(c), the signals at contact hole L and R disappeared although the A_{odd} and ϕ_{odd} signals were observed at the y-directional edges. Here, $\mathbf{I}_c$ flows only in the Co/Pt multilayer, and only $\mathbf{J}_{q,AEE}$ contributes to the LIT signal. Therefore, the LIT signals at the contact holes can be explained by the AHE-driven Peltier effect by the following scenario [Figs. 3(b) and 3(d)]. First, AHE induces the transverse $\mathbf{E}_{AHE}$ along the $-x$ direction for the configuration of $\mathbf{I}_c \| -y$ and $\mathbf{M} \| +z$ due to the positive anomalous Hall angle in Co/Pt systems [Fig. 2(b)]. Consequently, the AHE-induced transverse charge current $\mathbf{J}_A$ flows from the Co/Pt multilayer into the Si layer through the Ta/Au contact at contact hole L, whereas it flows from Si into Co/Pt at contact hole R. Since *n*-type Si exhibits a much larger negative Seebeck coefficient than Ta and Au, such $\mathbf{J}_A$ flow generates heat release (absorption) at contact hole L (R) due to the Peltier effect. Although the AHE-driven Peltier effect and AEE exhibits identical symmetry and sign of temperature modulation, our series of experiments has revealed the capability of local cooling and heating for the transverse thermoelectric conversion originating from the interplay between AHE and the Peltier effect.

Finally, we investigate the characteristics of the temperature modulation induced by the AHE-driven Peltier cooling–heating in our Co/Pt–Si device. Figure 4(a) represents the A_{odd} and ϕ_{odd} images for the cross-shaped $[Co/Pt]_{12}$ multilayer on the SiO_x/Si substrate with contact holes at f = 25.0 Hz for various I_c values and Figure 4(b) shows the I_c dependence of the corresponding A_{odd} and ϕ_{odd} values at contact hole L and R (see also supplementary material S2 for the f dependence and comparison with the signal at the edge of wire). The magnitude of A_{odd} monotonically increased with the increase in I_c; however, it deviated from linearity, with a reduced slope of A_{odd} v.s. I_c at larger I_c values. This trend does not follow the linear-response behavior expected for the Peltier effect. To confirm its origin, we measured the current-voltage (*I*-*V*) characteristics of the connection of the Si substrate and Ta/Au electrodes by etching the Co/Pt multilayer using Ar ion milling [Fig. 5(a)]. As shown in Fig. 5(b), the *I*-*V* curve exhibited two distinct regimes: a linear region with a steep increase in I at low bias V, and a region above V = 0.2 V where the slope becomes markedly reduced and gradually varies with V increasing. Such behavior differs from that of a conventional ohmic conductor, in which a single linear relationship is expected over the entire voltage range. To further clarify this behavior, we calculated a well-known indicator of the conduction mechanism: $\alpha = d(\ln I)/d(\ln V)$, the local power-law exponent in the *I*-*V* curve on a double-logarithmic scale.[45–47] Figure 5(c) plots α as a function of V. In the region of $V < 0.2$ V, $\alpha \sim 0.9$, which is close to, but slightly smaller than, unity, corresponding to quasi-ohmic conduction. In contrast, α decreases below unity at higher V, suggesting a deviation from simple ohmic transport. This behavior may reflect the influence of contact resistance due to non-ideal ohmic contact and/or the intrinsic conductivity of the Si substrate. Regarding the latter, it is possible that carrier velocity saturation at high electric field reduces the effective mobility in our *n*-type Si, leading to sublinear increase in I with V increasing. Considering that the anomalous Hall angle of the Co/Pt multilayer is 3.7% and the maximum I_c value for the LIT measurements is 80 mA, the corresponding $\mathbf{J}_A$ is expected to lie within high-bias V range (> 1 V) in Fig. 5(b), which accounts for the observed deviation from linearity between A_{odd} and I_c [Fig. 4(b)]. This nonlinear behavior could be improved by replacing the semiconducting Si with a thermoelectric material that exhibits high electrical conductivity and by optimizing the interfacial contact resistance.

In summary, we have experimentally demonstrated the inverse process of Seebeck-effect-driven AHE: allocated temperature modulation induced by the AHE-driven Peltier effect without applying an external magnetic field using the Co/Pt multilayer and Si hybrid system. Infrared imaging with comparison of the temperature modulations between the devices with and without contact holes clearly justifies AHE-driven Peltier cooling–heating free from the conventional transverse magneto-thermoelectric contributions such as AEE. These results establish the AHE-driven Peltier effect as a previously unexplored member of the transverse thermoelectrics. However, the observed temperature change remains relatively small. This limitation may be addressed through several possible approaches as is the case with Seebeck-effect-driven AHE. The first is to employ an all-bulk structure using bulk magnetic materials. Previous studies on Seebeck-effect-driven AHE have been demonstrated in all-bulk systems, suggesting the feasibility of this strategy. The use of bulk magnetic materials would allow much larger $\mathbf{J}_A$ to be injected through the contacts owing to the decrease in their electrical resistance, which will dramatically enhance the thermoelectric temperature modulation. The second approach is to improve the relevant transport parameters, particularly the difference in the Peltier coefficient between two materials and the Hall angle. For the latter, $\mathbf{J}_A$ is limited by the Hall angle relative to $\mathbf{I}_c$, the resulting temperature modulation is only a few percent of that achievable by conventional Peltier cooling in the present system. However, materials exhibiting anomalous/ordinary Hall angles of several tens or even hundreds of percent have recently been reported,[48–50] enabling more efficient induction of $\mathbf{J}_A$. In addition, optimizing the size ratio between the magnetic and thermoelectric components,[51] as well as the overall device structure design including the selection of contact electrodes and interface engineering to improve charge current injection and/or thermal confinement, would further enhance the transverse thermoelectric performance for specific applications. These directions should open a route toward the realization of more efficient Hall-effect-based allocative thermal management.

See the supplementary material for more information on the steady-state temperature during the LIT measurements and f dependence of the LIT signals.

The authors thank S. J. Park, T. Itoh, and T. Imamura for their technical support and valuable discussions. This work was supported by the ERATO "Magnetic Thermal Management Materials Project" (No. JPMJER2201) from JST, Japan; the Grant-in-Aid for Early-Career Scientists (No. 25K17940), Grant-in-Aid for Scientific Research (C) (No. 25K08463), and Grant-in-Aid for Scientific Research (S) (No. 22H04965) from JSPS KAKENHI, Japan. AR was supported by Prime Minister's Research Fellowship (PMRF), India.

AUTHOR DECLARATIONS

Conflict of Interest

The authors have no conflicts to disclose.

Author Contributions

Aritra Ray: Data curation (lead); Formal analysis (lead); Resources (equal); Writing – original draft (supporting).

Takamasa Hirai: Conceptualization (equal); Data curation (equal); Formal analysis (equal); Funding acquisition (equal); Investigation (lead); Methodology (lead); Resources (equal); Visualization (lead); Writing – original draft (lead); Writing – review & editing (lead).

Weinan Zhou: Data curation (equal); Investigation (equal); Methodology (equal); Resources (equal); Visualization (equal); Writing – original draft (supporting); Writing – review & editing (supporting).

Nanhe Kumar Gupta: Data curation (supporting); Writing – review & editing (supporting).

Yuya Sakuraba: Resources (supporting); Supervision (equal); Writing – review & editing (supporting).

Ken-ichi Uchida: Conceptualization (lead); Funding acquisition (lead); Investigation (supporting); Methodology (supporting); Resources (equal); Supervision (lead); Writing – original draft (equal); Writing – review & editing (supporting).

DATA AVAILABILITY

The data that support the findings of this study are available from the corresponding authors upon reasonable request.

REFERENCES

[1]M. H. Elsheikh, D. A. Shnawah, M. F. M. Sabri, S. B. M. Said, M. H. Hassan, M. B. Ali Bashir, and M. Mohamad, Renew. Sustain. Energy Rev. **30**, 337 (2014).
[2]T. Hendricks, T. Caillat, and T. Mori, Energies **15**, 7307 (2022).
[3]Q. Yan and M. G. Kanatzidis, Nat. Mater. **21**, 503 (2022).
[4]T. J. Seebeck, *Magnetische Polarisation Der Metalle Und Erze Durch Temperatur-Differenz* (Abh. Preuss. Akad. Wiss., 1822).
[5]J. C. A. Peltier, *Nouvelles Expériences Sur La Caloricité Des Courants Électrique.*, Vol. 56 (Ann. Chim. Phys., 1834).
[6]L. E. Bell, Science **321**, 1457 (2008).
[7]K. Uchida, W. Zhou, and Y. Sakuraba, Appl. Phys. Lett. **118**, 140504 (2021).
[8]K. Uchida and J. P. Heremans, Joule **6**, 2240 (2022).
[9]A. Sakai and S. Nakatsuji, Sci. Technol. Adv. Mater. **26**, 2554047 (2025).
[10]H. Adachi, F. Ando, T. Hirai, R. Modak, M. A. Grayson, and K. Uchida, Appl. Phys. Express **18**, 090101 (2025).
[11]W. Zhou and Y. Sakuraba, Appl. Phys. Express **13**, 043001 (2020).
[12]T. Higo, Y. Li, K. Kondou, D. Qu, M. Ikhlas, R. Uesugi, D. Nishio-Hamane, C. L. Chien, Y. Otani, and S. Nakatsuji, Adv. Funct. Mater. **31**, 2008971 (2021).
[13]M. Murata, K. Nagase, K. Aoyama, A. Yamamoto, and Y. Sakuraba, iScience **24**, 101967 (2021).
[14]R. Modak, Y. Sakuraba, T. Hirai, T. Yagi, H. Sepehri-Amin, W. Zhou, H. Masuda, T. Seki, K. Takanashi, T. Ohkubo, and K. Uchida, Sci. Technol. Adv. Mater. **23**, 767 (2022).
[15]H. Tanaka, T. Higo, R. Uesugi, K. Yamagata, Y. Nakanishi, H. Machinaga, and S. Nakatsuji, Adv. Mater. **35**, 2303416 (2023).
[16]F. Ando, T. Hirai, and K. Uchida, APL Energy 2, 016103 (2024).
[17]K. Uchida, T. Hirai, F. Ando, and H. Sepehri-Amin, Adv. Energy Mater. **14**, 2302375 (2024).
[18]T. Hirai, F. Ando, H. Sepehri-Amin, and K. Uchida, Nat. Commun. **15**, 9643 (2024).
[19]M. Odagiri, H. Imaeda, A. Yagmur, Y. Kurokawa, S. Sumi, H. Awano, and K. Tanabe, Sci. Rep. **14**, 17205 (2024).

[20]M. Murata, T. Hirai, T. Seki, and K. Uchida, Appl. Phys. Lett. **124**, 193901 (2024).
[21]M. Chen, J. Wang, K. Liu, W. Fan, Y. Sun, C. Felser, T. Zhu, and C. Fu, Adv. Energy Mater. **14**, 2400411 (2024).
[22]S. Ota, K. Uchida, R. Iguchi, P. V. Thach, H. Awano, and D. Chiba, Sci. Rep. **9**, 13197 (2019).
[23]R. Das, R. Iguchi, and K. Uchida, Phys. Rev. Applied **11**, 034022 (2019).
[24]J. Wang, Y. K. Takahashi, and K. Uchida, Nat. Commun. **11**, 2 (2020).
[25]W. Zhou, K. Yamamoto, A. Miura, R. Iguchi, Y. Miura, K. Uchida, and Y. Sakuraba, Nat. Mater. **20**, 463 (2021).
[26]K. Yamamoto, R. Iguchi, A. Miura, W. Zhou, Y. Sakuraba, Y. Miura, and K. Uchida, J. Appl. Phys. **129**, 223908 (2021).
[27]W. Zhou, A. Miura, T. Hirai, Y. Sakuraba, and K. Uchida, Appl. Phys. Lett. **122**, 062402 (2023).
[28]W. Zhou, T. Hirai, K. Uchida, and Y. Sakuraba, J. Phys. D: Appl. Phys. **55**, 335002 (2022).
[29]J. H. Park, C. Park, T. Jeong, M. T. Moneck, N. T. Nufer, and J. G. Zhu, J. Appl. Phys. **103**, 07A917 (2008).
[30]S. L. Zhang, J. Teng, J. Y. Zhang, Y. Liu, J. W. Li, G. H. Yu, and S. G. Wang, Appl. Phys. Lett. **97**, 222504 (2010).
[31]J. Y. Zhang, Z. L. Wu, S. G. Wang, C. J. Zhao, G. Yang, S. L. Zhang, Y. Liu, S. Liu, J. Teng, and G. H. Yu, Appl. Phys. Lett. **102**, 102404 (2013).
[32]S. L. Jiang, X. Chen, X. J. Li, K. Yang, J. Y. Zhang, G. Yang, Y. W. Liu, J. H. Lu, D. W. Wang, J. Teng, and G. H. Yu, Appl. Phys. Lett. **107**, 112404 (2015).
[33]S. L. Jiang, G. Yang, J. Teng, Q. X. Guo, L. L. Li, and G. H. Yu, Appl. Surf. Sci. **387**, 375 (2016).
[34]T. Hirai, T. Koyama, A. Obinata, Y. Hibino, K. Miwa, S. Ono, M. Kohda, and D. Chiba, Appl. Phys. Express **9**, 063007 (2016).
[35]T. Hirai, T. Koyama, and D. Chiba, Appl. Phys. Lett. **112**, 122408 (2018).
[36]S. Daimon, R. Iguchi, T. Hioki, E. Saitoh, and K. Uchida, Nat. Commun. **7**, 13754 (2016).
[37]S. Daimon, K. Uchida, R. Iguchi, T. Hioki, and E. Saitoh, Phys. Rev. B **96**, 024424 (2017).
[38]Y. Hirayama, R. Iguchi, X.F. Miao, K. Hono, and K. Uchida, Appl. Phys. Lett. **111**, 163901 (2017).
[39]T. Seki, R. Iguchi, K. Takanashi, and K. Uchida, Appl. Phys. Lett. **112**, 152403 (2018).
[40]K. Uchida, M. Murata, A. Miura, and R. Iguchi, Phys. Rev. Lett. **125**, 106601 (2020).
[41]T. Hirai, R. Iguchi, A. Miura, and K. Uchida, Adv. Funct. Mater. **32**, 2201116 (2022).
[42]T. Imamura, T. Hirai, W. Zhou, Y. Sakuraba, and K. Uchida, Appl. Phys. Lett. **127**, 102401 (2025).
[43]Y. Zhang, Q. Jiang, J. Yang, M. Lv, Q. Li, D. Hou, and J. Wang, Int. J. Therm. Sci. **220**, 110357 (2026).
[44]H. Nakayama, T. Hirai, J. Uzuhashi, R. Iguchi, T. Ohkubo, T. Koyama, D. Chiba, and K. Uchida, Appl. Phys. Express **12**, 123003 (2019).
[45]L. Wang, C. Yang, J. Wen, S. Gai, and Y. Peng, J. Mater. Sci.: Mater. Electron. **26**, 4618 (2015).
[46]T. Guo, K. Pan, Y. Jiao, B. Sun, C. Du, J. P. Mills, Z. Chen, X. Zhao, L. Wei, Y. N. Zhou, and Y. A. Wu, Nanoscale Horiz. **7**, 299 (2022).
[47]S. Cruces, M. D. Ganeriwala, J. Lee, K. Ran, J. Jo, L. Völkel, D. Braun, B. Canto, E. G. Marín, H. Kalisch, M. Heuken, A. Vescan, R. E. Dunin-Borkowski, J. Mayer, A. Godoy, A. Daus, and M. C. Lemme, Nano Lett. **25**, 12455 (2025).
[48]A. K. Nayak, J. E. Fischer, Y. Sun, B. Yan, J. Karel, A. C. Komarek, C. Shekhar, N. Kumar, W. Schnelle, J. Kübler, C. Felser, and S. S. P. Parkin, Sci. Adv. **2**, e1501870 (2016).

[49]E. Liu, Y. Sun, N. Kumar, L. Muechler, A. Sun, L. Jiao, S.Y. Yang, D. Liu, A. Liang, Q. Xu, J. Kroder, V. Süß, H. Borrmann, C. Shekhar, Z. Wang, C. Xi, W. Wang, W. Schnelle, S. Wirth, Y. Chen, S. T. B. Goennenwein, and C. Felser, Nat. Phys. **14**, 1125 (2018).
[50]S. L. Bud'ko, S. Huyan, and P. C. Canfield, Phys. Rev. B **113**, 014431 (2026).
[51]K. Yamamoto, R. Iguchi, A. Miura, W. Zhou, Y. Sakuraba, Y. Miura, and K. Uchida, J. Appl. Phys. **130**, 039901 (2021).

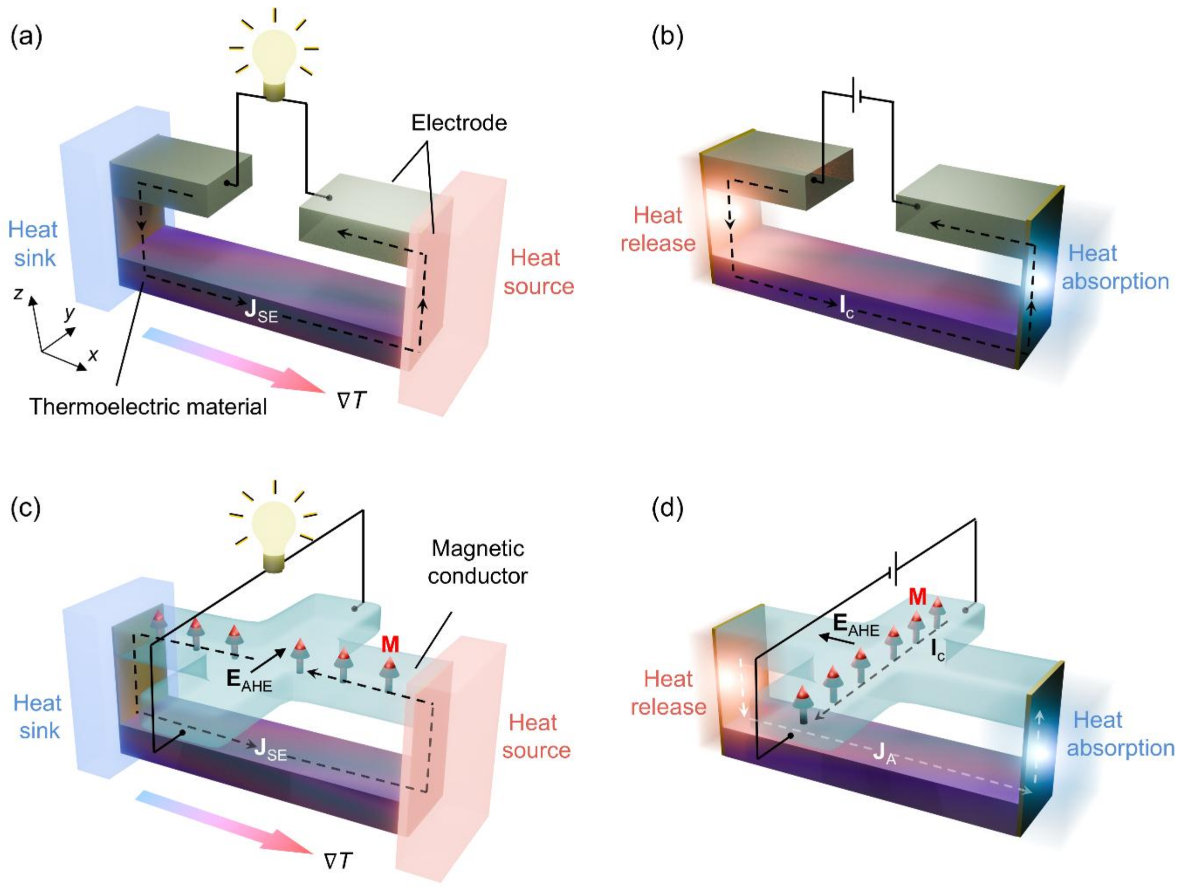

FIG 1. (a),(b) Schematic illustrations of the Seebeck effect (a) and Peltier effect (b). ∇T, $\mathbf{J}_{SE}$, and $\mathbf{I}_c$ denote the applied temperature gradient, charge current generated by the Seebeck effect, and applied charge current, respectively. In (a)[(b)], ∇T ($\mathbf{I}_c$) along the x axis induces $\mathbf{J}_{SE}$ (heat current) in the same axis, resulting the longitudinal thermoelectric voltage generation (temperature modulation). (c),(d) Schematic illustration of the Seebeck-effect-driven anomalous Hall effect (AHE) (c) and AHE-driven Peltier effect (d). $\mathbf{M}$, $\mathbf{E}_{AHE}$, and $\mathbf{J}_A$ represent the magnetization, AHE-induced electric field, and transverse charge current induced by $\mathbf{E}_{AHE}$, respectively. In (c), ∇T along the x axis induces $\mathbf{J}_{SE}$, which flows through a magnetic conductor magnetized along the z axis. Owing to AHE, $\mathbf{E}_{AHE}$ is generated along the y axis, resulting in the transverse thermoelectric voltage generation. Conversely, in (d), $\mathbf{I}_c$ along the y axis generates transverse $\mathbf{E}_{AHE}$ along the x axis via AHE, thereby inducing $\mathbf{J}_A$ flow into the thermoelectric material, and giving rise to temperature modulation at the junction through the Peltier effect.

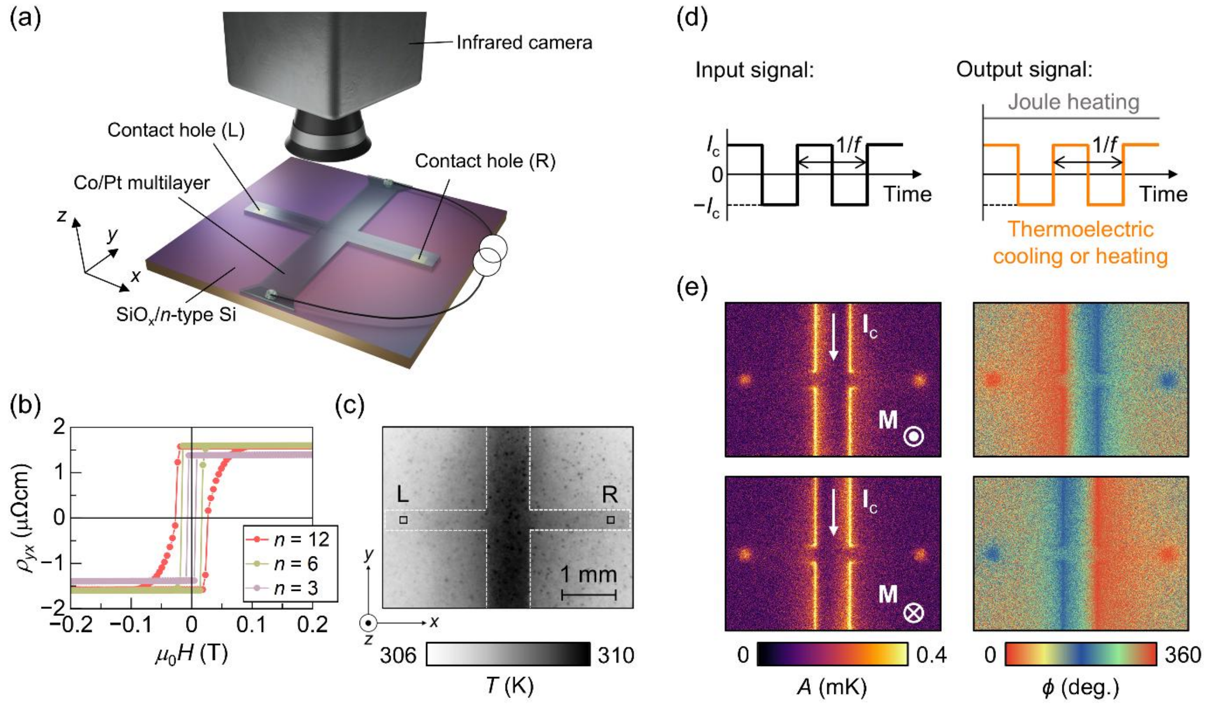

FIG 2. (a) Schematic of experimental set-up for lock-in thermography (LIT) measurement. (b) Magnetic field H dependence of Hall resistivity ρ_{yx} of $[Co/Pt]_n$ multilayers with n = 3, 6, and 12. (c) Steady-state infrared image with temperature T for the cross-shaped $[Co/Pt]_{12}$ multilayer on the SiO_x/Si substrate during the LIT measurement at I_c = 80 mA. White dashed line shows the wire of the $[Co/Pt]_{12}$ multilayer and L and R with black squares represent the position of contact holes. (d) Time charts of the input charge current and output temperature changes induced by thermoelectric effects and Joule heating. I_c and f denote the amplitude and frequency of the square-wave-modulated ac charge current. (e) Lock-in amplitude A and phase ϕ images at I_c = 80 mA and f = 25 Hz when **M** of the $[Co/Pt]_{12}$ multilayer aligned along the $+z$ (top panels) and $-z$ (bottom panels) directions.

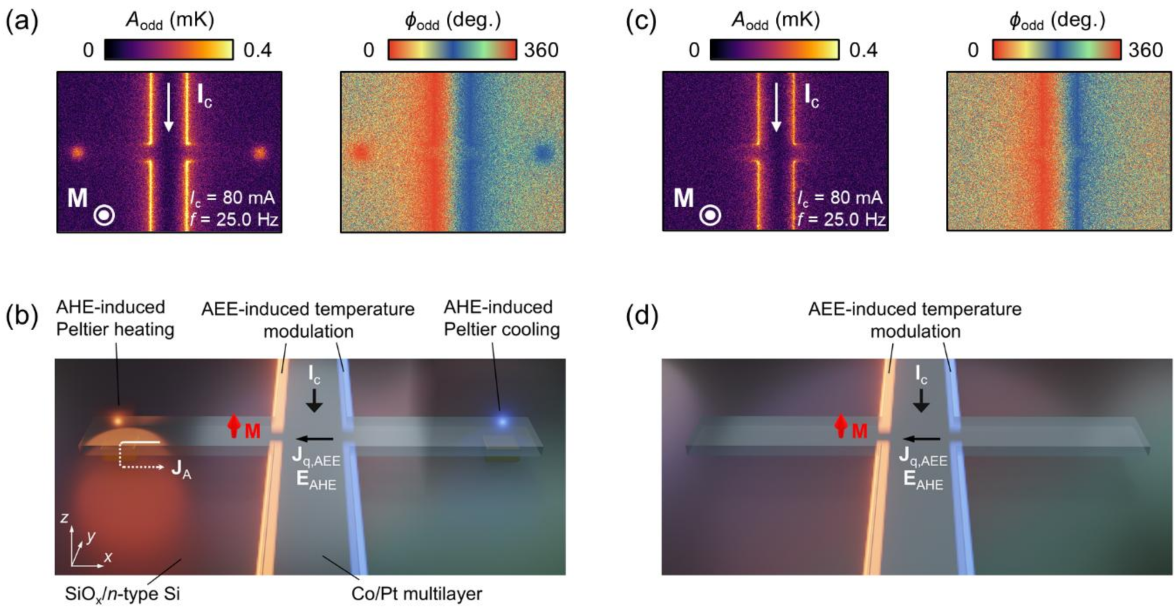

FIG 3. (a) **M**-odd-dependent A and ϕ (A_{odd} and ϕ_{odd}, respectively) images for the $[\mathrm{Co/Pt}]_{12}$ multilayer on the $\mathrm{SiO_x/Si}$ substrate with Ta/Au contact holes at I_c = 80 mA and f = 25 Hz. (b) Schematic for the temperature modulation induced by the AHE-induced Peltier effect and anomalous Ettingshausen effect. (c),(d) LIT result and schematic illustration for the $[\mathrm{Co/Pt}]_{12}$ multilayer on the Si substrate without contact holes.

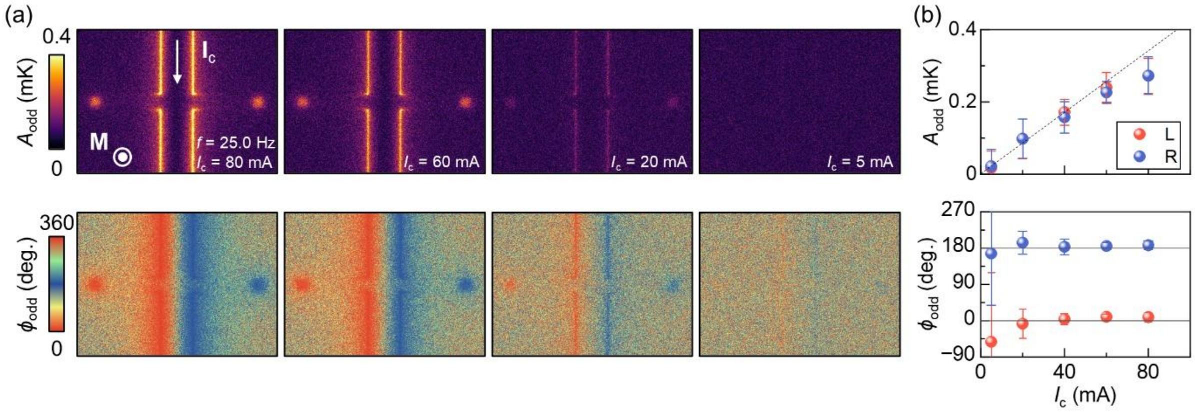

FIG 4. (a) A_{odd} and ϕ_{odd} images for the $[\mathrm{Co/Pt}]_{12}$ multilayer on the $\mathrm{SiO_x/Si}$ substrate with Ta/Au contact holes at f = 25 Hz for various I_{c} values. (b) I_{c} dependence of the A_{odd} and ϕ_{odd} signals at contact holes L (red) and R (blue). The data points in (b) were obtained by averaging the A_{odd} and ϕ_{odd} values on the areas defined by the squares shown in Fig. 2(c). The dotted line in the A_{odd} plot of (b) shows the result of linear fitting using the A_{odd} data at I_{c} = 5, 20, and 40 mA as a guide for confirming the deviation of linearity at large I_{c}.

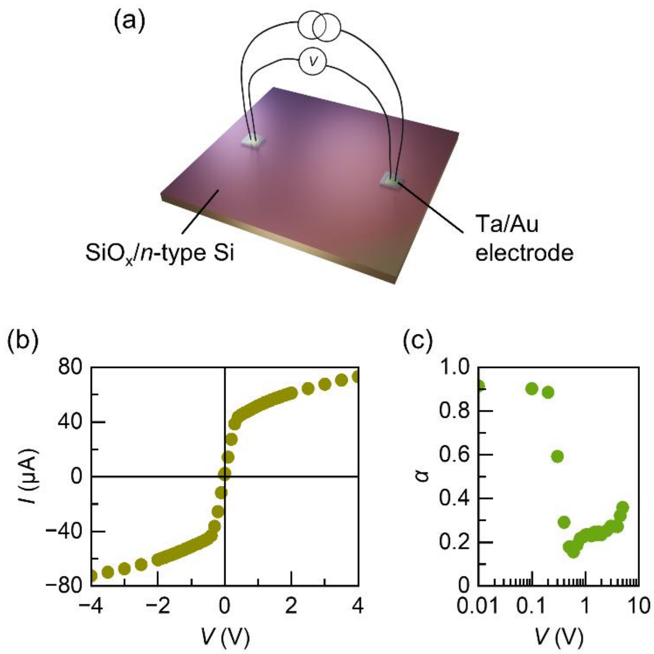

FIG 5. (a) Schematic of the measurement configuration of current-voltage (*I*-*V*) characteristic of the Si substrate and Ta/Au electrodes. (b) *I*-*V* curve. (c) *V* dependence of $\alpha = d(\ln I)/d(\ln V)$.